IOP Publishing Journal of Physics B: Atomic, Molecular and Optical Physics

J. Phys. B: At. Mol. Opt. Phys. **40** (2007) 4391–4402 doi:10.1088/0953-4075/40/22/008

The evolution of the triple differential cross sections for the double photoionization of He and H_2

J Colgan[1], M Foster[1], M S Pindzola[2] and F Robicheaux[2]

[1] Theoretical Division, Los Alamos National Laboratory, Los Alamos, NM 87545, USA
[2] Department of Physics, Auburn University, Auburn, AL 36849, USA

Received 20 August 2007, in final form 17 September 2007
Published 5 November 2007
Online at stacks.iop.org/JPhysB/40/4391

Abstract

We use the time-dependent close-coupling method to explore the triple differential cross sections produced by double photoionization of He and H_2. Recent extensions of our technique have allowed extraction of the triple differential cross section as the double photoionization process evolves, allowing further exploration of the underlying mechanisms. We demonstrate that the angular distributions of the two outgoing electrons typically reach a converged shape after 5 or 6 field periods. We also further compare our method with recent experimental measurements, as well as demonstrating some similarities in the triple differential cross sections for He and for H_2 at certain molecular orientations.

(Some figures in this article are in colour only in the electronic version)

1. Introduction

Investigations of the double photoionization of light, two-electron systems, such as He and H_2, have long been an attractive choice for study by both theoretical and experimental atomic collision physics. The three-body nature of the problem allows detailed investigations of the interactions between the outgoing electrons as they escape the Coulomb potential of the atomic or molecular ion. In the last ten years theory and experiment have consistently found very good agreement for all possible measurable quantities for the double photoionization of He. A variety of time-independent and time-dependent theories [1–9] show good agreement with each other, and with experiment (e.g. [10]), for total, single, double and triple differential cross sections for a variety of photon energies, and outgoing electron energies and angles.

For the more difficult molecular case, it is only within the last couple of years that theoretical developments have allowed fully *ab initio* calculations of the double photoionization of H_2. Recently, the time-independent exterior-complex-scaling (ECS) method [11, 12] and the time-dependent close-coupling method (TDCC) [13] have demonstrated excellent agreement with each other and with recent measurements of the triple differential cross sections for this process [14–16]. Both methods had previously been

shown to also give accurate total double photoionization cross sections [17, 18]. These studies have also been able to uncover some interesting dynamical effects unique to the molecular ionization case [19].

In this paper, we strive to uncover some of the behaviour of the electrons as they leave the atom or molecule using the time-dependent close-coupling method. Examples are presented for both double photoionization of He and H_2 and for various energy sharings between the outgoing electrons. We caution that this study explores the time history of the triple differential cross sections, and is not an investigation of how the photoionization process changes as a result of differing pulse lengths. In this study, the electromagnetic field is always on, and the angular distributions are extracted at earlier times during the photoionization process.

2. Theory

The development of the time-dependent close-coupling method for double photoionization of He [5–7] and H_2 [13, 18] has previously been described in detail. Here we give only a brief summary, comparing the approaches for the atomic and molecular cases.

The time-dependent Schrödinger equation for photoionization of He or H_2 [5], in the weak-field limit, can be written as

$$\mathrm{i}\frac{\partial\psi(\vec{r}_1,\vec{r}_2,t)}{\partial t} = H\psi(\vec{r}_1,\vec{r}_2,t) + V\psi_0(\vec{r}_1,\vec{r}_2)\,\mathrm{e}^{-\mathrm{i}E_0t}, \tag{1}$$

where H is the atomic or molecular Hamiltonian, V is the time-dependent radiation field Hamiltonian and ψ_0 and E_0 are the exact eigenfunction and eigenenergy of the atomic or molecular ground state. In the atomic case, the total wavefunction Ψ may be expanded in coupled spherical harmonics as

$$\psi(\vec{r}_1,\vec{r}_2,t) = \sum_{l_1l_2}\frac{P^L_{l_1l_2}(r_1,r_2,t)}{r_1r_2}Y^L_{l_1l_2}(\vec{r}_1,\vec{r}_2), \tag{2}$$

where $Y^L_{l_1l_2}(\vec{r}_1,\vec{r}_2)$ is a coupled spherical harmonic, and in the molecular case the total wavefunction may be expanded in products of rotation functions [18] as

$$\psi(\vec{r}_1,\vec{r}_2,t) = \sum_{m_1,m_2}\frac{P^M_{m_1m_2}(r_1,\theta_1,r_2,\theta_2,t)}{r_1r_2\sqrt{\sin\theta_1}\sqrt{\sin\theta_2}}\Phi_{m_1}(\phi_1)\Phi_{m_2}(\phi_2). \tag{3}$$

Here, $\Phi_m(\phi) = \frac{\mathrm{e}^{\mathrm{i}m\phi}}{\sqrt{2\pi}}$ and $M = m_1 + m_2$ is the projection of total electronic angular momentum onto the z-axis. Substitution of these expansions into equation (1) yields a set of time-dependent close-coupled partial differential equations given by

$$\begin{aligned}\mathrm{i}\frac{\partial P^L_{l_1l_2}(r_1,r_2,t)}{\partial t} &= T_{l_1l_2}(r_1,r_2)P^L_{l_1l_2}(r_1,r_2,t) + \sum_{l_1',l_2'}V^L_{l_1l_2,l_1'l_2'}(r_1,r_2)P^L_{l_1'l_2'}(r_1,r_2,t)\\ &\quad + \sum_{l_1'',l_2''}W^{LL_0}_{l_1l_2,l_1''l_2''}(r_1,r_2,t)\bar{P}^{L_0}_{l_1''l_2''}(r_1,r_2)\,\mathrm{e}^{-\mathrm{i}E_0t},\end{aligned} \tag{4}$$

for the atomic case, and by

$$\begin{aligned}\mathrm{i}\frac{\partial P^M_{m_1m_2}(r_1,\theta_1,r_2,\theta_2,t)}{\partial t} &= T_{m_1m_2}(r_1,\theta_1,r_2,\theta_2)P^M_{m_1m_2}(r_1,\theta_1,r_2,\theta_2,t)\\ &\quad + \sum_{m_1',m_2'}V^M_{m_1m_2,m_1'm_2'}(r_1,\theta_1,r_2,\theta_2)P^M_{m_1'm_2'}(r_1,\theta_1,r_2,\theta_2,t)\\ &\quad + \sum_{m_1'',m_2''}W^{MM_0}_{m_1m_2,m_1''m_2''}(r_1,\theta_1,r_2,\theta_2,t)\bar{P}^{M_0}_{m_1''m_2''}(r_1,\theta_1,r_2,\theta_2)\,\mathrm{e}^{-\mathrm{i}E_0t},\end{aligned} \tag{5}$$

for the molecular case, where expressions for the various kinetic energy, one-electron potential, and two-electron potential terms may be found in [5, 18], and $\bar{P}^{L_0}_{l_1 l_2}$ and $\bar{P}^{M_0}_{m_1 m_2}$ are the reduced wavefunctions for ψ_0, for He and H_2 respectively. The exact lattice eigenfunction for the He or H_2 ground state is obtained by relaxation of the Schrödinger equation in imaginary time ($\tau = \mathrm{i}t$):

$$-\frac{\partial \psi_0(\vec{r}_1, \vec{r}_2, \tau)}{\partial \tau} = H\psi_0(\vec{r}_1, \vec{r}_2, \tau). \tag{6}$$

The wavefunction ψ_0 can again be expanded in products of coupled spherical harmonics or rotation functions and substituted into equation (6), yielding a set of close-coupled partial differential equations in space and imaginary time.

We solve the time-dependent close-coupling equations using lattice techniques to obtain a discrete representation of the reduced wavefunctions and all operators on a two-dimensional radial grid for the He calculations, and a four-dimensional radial and angular grid for the H_2 calculations. In the calculations presented here, similar grids were employed as used in previous studies [6, 13]. For the atomic two-dimensional calculations a 640-point grid was employed with a spacing of 0.1 au. Typically, eight terms were retained in the angular momentum expansion in equation (4). For the molecular four-dimensional calculations, a grid of $(384, 32)$ points was used with mesh spacings of 0.1 au and 0.03125π au for the radial and angular grids respectively. Typically, eight terms were retained in the expansions in equation (5). The coupled equations (4), (5) were propagated for usually 10 field periods.

The total cross section for double photoionization can be written as

$$\sigma_{\mathrm{dion}} = \frac{\omega}{I}\frac{\partial \mathcal{P}_{\mathrm{dion}}}{\partial t}, \tag{7}$$

where ω and I are the radiation field frequency and intensity respectively. We note that, in this approach, the radiation field is always present, and the double ionization cross section is found by taking the time derivative of the double ionization probability, which is always increasing. An alternative approach [20] is to subject the atom to a radiation pulse of given length and shape, in which case the double ionization cross section must be extracted in a different manner [21], although such calculations yield results that are very similar to the results presented in this paper. The double photoionization probability, $\mathcal{P}_{\mathrm{dion}}$, can be defined as

$$\mathcal{P}_{\mathrm{dion}} = \sum_{l_1 l_2} \int \mathrm{d}k_1 \int \mathrm{d}k_2 \left| P^L_{l_1 l_2}(k_1, k_2, t) \right|^2 \tag{8}$$

for He, and by

$$\mathcal{P}_{\mathrm{dion}} = \sum_{l_1 l_2} \sum_{m_1 m_2} \int \mathrm{d}k_1 \int \mathrm{d}k_2 \left| P^M_{l_1 m_1 l_2 m_2}(k_1, k_2, t) \right|^2, \tag{9}$$

for H_2. The momentum-space wavefunctions, $P^L_{l_1 l_2}(k_1, k_2, t)$ or $P^M_{l_1 m_1 l_2 m_2}(k_1, k_2, t)$, are defined as

$$P^L_{l_1 l_2}(k_1, k_2, t) = \int_0^\infty \mathrm{d}r_1 \int_0^\infty \mathrm{d}r_2 P^L_{l_1 l_2}(r_1, r_2, t) P_{k_1 l_1}(r_1) P_{k_2 l_2}(r_2), \tag{10}$$

and

$$\begin{aligned} P^M_{l_1 m_1 l_2 m_2}(k_1, k_2, t) = {} & \int_0^\infty \mathrm{d}r_1 \int_0^\pi \mathrm{d}\theta_1 \int_0^\infty \mathrm{d}r_2 \int_0^\pi \mathrm{d}\theta_2 \\ & P^M_{m_1 m_2}(r_1, \theta_1, r_2, \theta_2, t) P^*_{k_1 l_1 m_1}(r_1, \theta_1) P^*_{k_2 l_2 m_2}(r_2, \theta_2), \end{aligned} \tag{11}$$

respectively. In these equations $P_{kl}(r)$ and $P_{klm}(r,\theta)$ are continuum functions of He^+ or H_2^+ respectively, obtained by direct numerical integration of the time-independent Schrödinger equation [6]. The triple differential cross section for double photoionization of He or H_2 can now be written as

$$\frac{\mathrm{d}^3\sigma}{\mathrm{d}\alpha\,\mathrm{d}\Omega_1\mathrm{d}\Omega_2} = \frac{\omega}{I}\frac{\partial}{\partial t}\int \mathrm{d}k_1 \int \mathrm{d}k_2 \delta\left(\tan\alpha - \frac{k_2}{k_1}\right)|\mathcal{M}|^2, \tag{12}$$

where Ω_1 and Ω_2 are the solid angles in which the outgoing electrons are ejected (with $\Omega \equiv (\theta,\phi)$) with respect to the polarization axis. For He, the amplitude $\mathcal{M}$ is given by

$$\mathcal{M} = \sum_{l_1 l_2} (-\mathrm{i})^{l_1+l_2}\,\mathrm{e}^{\mathrm{i}(\sigma_{l_1}+\sigma_{l_2})} P^L_{l_1 l_2}(k_1,k_2,t) Y^L_{l_1 l_2}(\hat{k}_1,\hat{k}_2), \tag{13}$$

where $Y^L_{l_1 l_2}(\hat{k}_1,\hat{k}_2)$ is a coupled spherical harmonic. Similarly, for double photoionization of H_2, for the case where the polarization axis is oriented at an arbitrary solid angle (θ_N,ϕ_N) to the molecular internuclear distance, the amplitude $\mathcal{M}$ is given by

$$\begin{aligned}\mathcal{M} = \sum_{l_1 l_2}\sum_{m_1 m_2} (-\mathrm{i})^{l_1+l_2}\,\mathrm{e}^{\mathrm{i}(\sigma_{l_1}+\sigma_{l_2})} \Bigg\{ & \cos\theta_N P^{M=0}_{l_1 m_1 l_2 m_2}(k_1,k_2,t) Y_{l_1 m_1}(\hat{k}_1) Y_{l_2 m_2}(\hat{k}_2)\delta_{m_1+m_2,0} \\ & + \sin\theta_N \left[\frac{\cos\phi_N - \mathrm{i}\sin\phi_N}{\sqrt{2}}\right] P^{M=+1}_{l_1 m_1 l_2 m_2}(k_1,k_2,t) Y_{l_1 m_1}(\hat{k}_1) Y_{l_2 m_2}(\hat{k}_2)\delta_{m_1+m_2,1} \\ & + \sin\theta_N \left[\frac{\cos\phi_N + \mathrm{i}\sin\phi_N}{\sqrt{2}}\right] P^{M=-1}_{l_1 m_1 l_2 m_2}(k_1,k_2,t) Y_{l_1 m_1}(\hat{k}_1) Y_{l_2 m_2}(\hat{k}_2)\delta_{m_1+m_2,-1} \Bigg\},\end{aligned} \tag{14}$$

where in these equations σ_l is the Coulomb phase and $Y_{lm}(\hat{k})$ represents a spherical harmonic.

3. Results and discussion

Comparison of the computed triple differential cross sections for He and H_2 with experiment is usually made by extracting the momentum-space wavefunctions $P(k_1,k_2,t)$ at some long time which is usually 10 field periods or more. This approach has yielded excellent agreement between TDCC calculations for He [6, 7] and H_2 [13] with experiment [10, 16] for a range of outgoing electron energies and angles. As a further example of such agreement, in figures 1 and 2 we compare TDCC calculations for double photoionization of H_2 with recent relative experimental measurements of Weber *et al* [14, 15]. The measurements have been normalized to the TDCC calculations, with the same relative normalization used in each figure. Figure 1 shows measurements made when one of the electrons is ejected perpendicular to the plane defined by the polarization axis and the momentum vector of the second ejected electron, for various orientations of the molecule with respect to the polarization axis of the light (which is along the z axis). The electrons share the excess photon energy of 25 eV equally. The calculations, when averaged over the experimental uncertainties of the molecular and electron angles, and electron energies, are in good agreement with the measurements.

Figure 2 shows measurements made for the same electron ejection angles and for a fixed molecular orientation, for different kinetic energy release (KER) of the outgoing protons. By measuring the kinetic energy imparted to the protons, one can infer the internuclear separation of the molecule at the time of double photoionization. In this case, the measurements are compared with TDCC calculations made at different internuclear separations, which correspond to the average KER of the protons. Again, the agreement between theory and

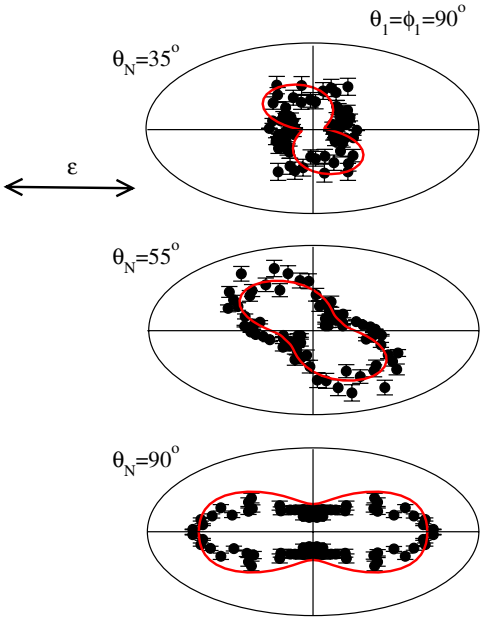

Figure 1. Triple differential cross sections for H_2 for $E_1 = E_2 = 12.5$ eV, for one electron ejected perpendicular to the plane defined by the polarization axis and the momentum vector of the second ejected electron, and for various angles of the molecule with respect to the polarization axis, as indicated. The TDCC calculations (red lines) are compared to the measurements of Weber *et al* [15].

experiment is good, apart from the extra structure in the experimental data in the lower panel of figure 2, which is not seen in the calculations. We have checked the convergence of our calculations with respect to additional terms in the summations in equations (3) and (12) and found our results to be well converged. We also note that time-independent ECS calculations [19] did not show extra structure in the lower panel of figure 2.

It can also be instructive to extract the momentum-space wavefunction $P(k_1, k_2, t)$ at earlier times, during the photoionization process, in an effort to gain some insight into the double photoionization mechanisms. In figure 3 we revisit the double photoionization of He at a photon energy of 99 eV. The triple differential cross sections for equal electron energy sharing, and for the case where $\theta_1 = 0^\circ$, are extracted at nine different times during the double photoionization process from $2T$ to $10T$, where $T = 2\pi/\omega$ is the field period. At the final time $10T$ we compare the calculation to measurements of Bräuning *et al* [10] and find excellent agreement, as previously shown in [6]. There are several points of interest in the shapes of the angular distributions as time increases. The zero in the cross section at $\theta_2 = 180^\circ$ is present at all times. This arises from the selection rules which exist for double photoionization of He at equal energy sharing, as discussed by Maulbetsch and Briggs [22]. This zero in the cross section arises from the selection rule 'C' (as defined by [22]), which states that for $\mathbf{k}_1 = -\mathbf{k}_2$ singlet states with odd parity do not contribute to the cross section. However, the other zero in the cross section, at $\theta_2 = 0^\circ$, takes some time to form. In fact, at early times the cross sections are actually largest around $\theta_2 = 0^\circ$, which implies that the electrons are doubly ionized in similar directions, but that the electron–electron repulsion quickly pushes the electrons apart. After around 8 field periods, the shape and magnitude of the triple differential cross section is stable. This behaviour of the cross section as a function of time will have some slight

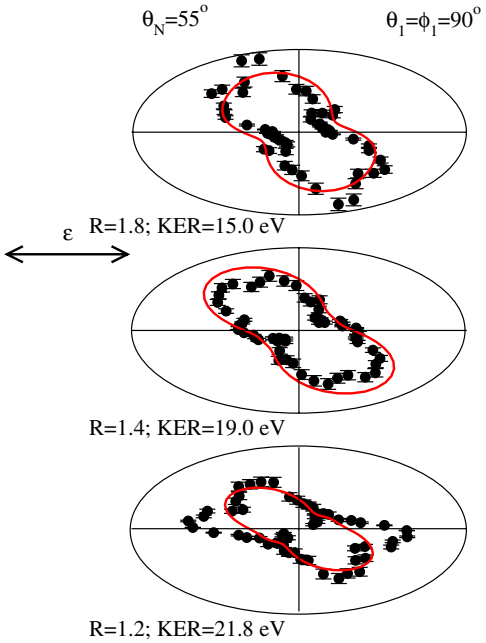

Figure 2. Triple differential cross sections for H_2 for equal electron energy sharing, for one electron ejected perpendicular to the plane, at a molecular angle of 55° with respect to the polarization axis, for various kinetic energy sharings between the outgoing protons. These correspond to various internuclear separations of the molecule at the time of double ionization, as indicated. The TDCC calculations (red lines) are compared to the measurements of Weber *et al* [15].

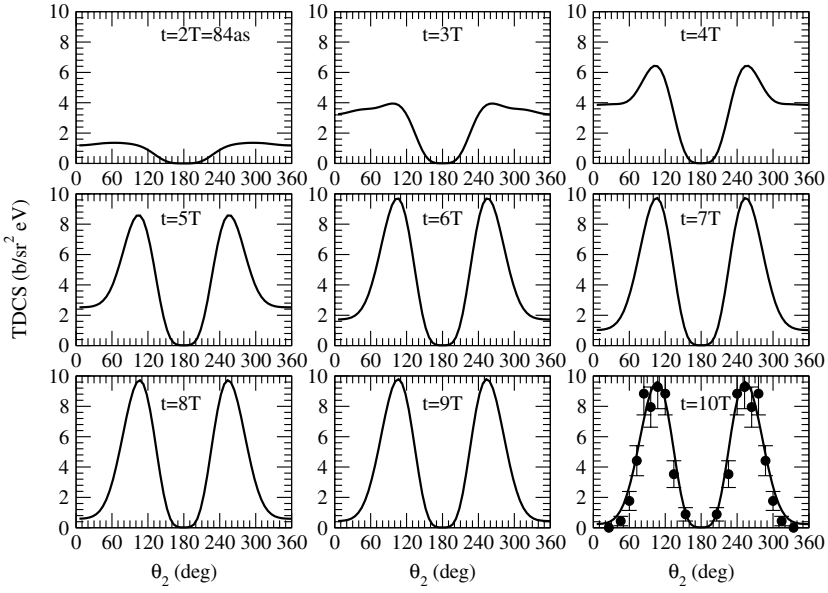

Figure 3. Triple differential cross sections for He for $E_1 = E_2 = 10$ eV, for $\theta_1 = 0°$. The differential cross sections are presented as a function of the number of field periods (T) elapsed during the propagation. The first cross sections are computed after 84 attoseconds (as) as indicated. At the final time of $10T$, we compare our calculations with the measurements of Bräuning *et al* [10].

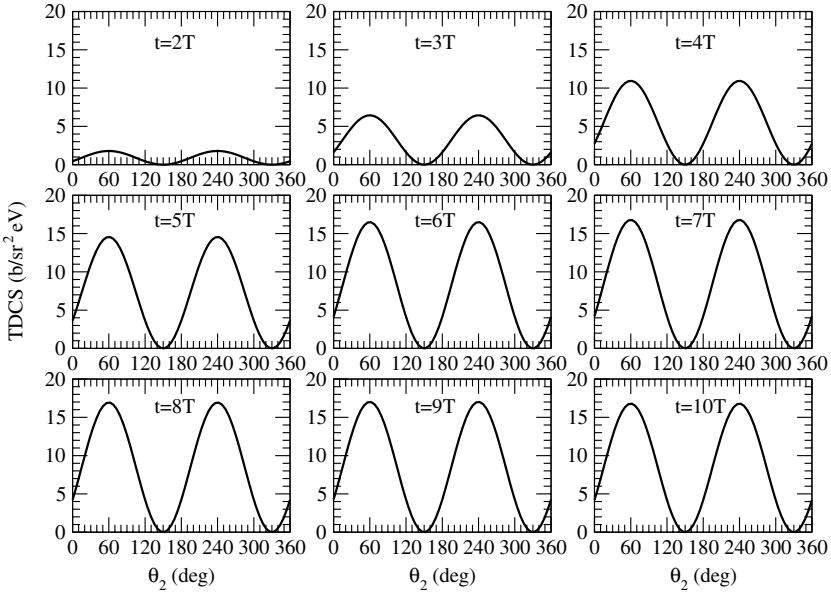

Figure 4. Triple differential cross sections for He for $E_1 = E_2 = 10$ eV, for $\theta_{12} = 120^\circ$. The differential cross sections are presented as a function of the number of field periods (T) elapsed during the propagation.

dependence on how the electric field is ramped on in the calculation (usually the electric field is ramped on over one quarter of a field period), but the broad behaviour is still the same. We also note that the magnitude of the cross sections increases until around 5 field periods, after which it is relatively constant. This reflects the increase in the magnitude of the total cross section, which has the same behaviour. The triple differential cross section shape at early times may lend further support to the model of a 'knock-out' mechanism for double photoionization at relatively low photon energies, which has previously been proposed (e.g. [23]). If double ionization proceeds via a binary collision, one might expect them to be ejected in similar directions before their mutual repulsion forces the electrons apart.

In figure 4 we show similar triple differential cross sections, where in this case the angle between the ejected electrons (θ_{12}) is kept fixed at 120°. Since in this case the electron–electron repulsion is kept constant at each time (since we extract the cross sections only for fixed θ_{12}), the shape of the triple differential cross section is not affected by the electron–electron repulsion. Instead, the shape is dominated at all times by the 'hard' selection rules [22], which give rise to the zeros in the cross section at $\theta_2 = 150^\circ$ and $\theta_2 = 330^\circ$. Again, the magnitude of the cross section rises and then levels off after around 5 or 6 field periods.

In figures 5 and 6 we show triple differential cross sections for H_2, again for equal energy sharing (in this case $E_1 = E_2 = 12.5$ eV), and again for $\theta_1 = 0^\circ$. In figure 5 the angle between the molecule and polarization axis is 90° (which implies that only the $M = 1$ final state contributes to ionization), and in figure 6 the angle between molecule and polarization axis is 0° (only $M = 0$ contributes to the ionization process). Figure 5 shows many similarities to the corresponding He case (figure 3), which may reflect the dominance of the final-state correlations in dictating the shape of the angular distributions. Similar selection rules to those discussed for He specify a zero in the cross section at $\theta_2 = 180^\circ$, and the zero formed at $\theta_2 = 0^\circ$ takes some time to develop. At the final time of $10T$, our TDCC calculations are

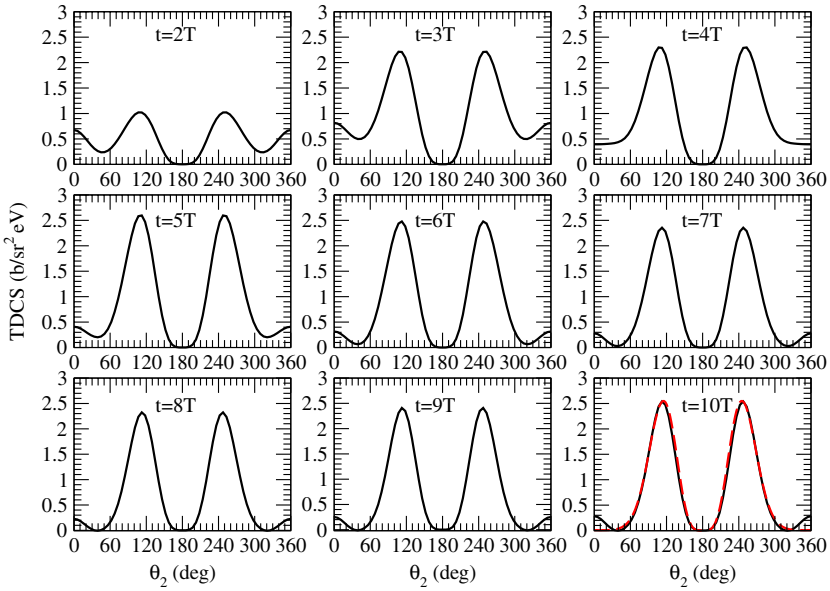

Figure 5. Triple differential cross sections for H_2 for $E_1 = E_2 = 12.5$ eV, for $\theta_1 = 0^\circ$, and for $\theta_N = 90^\circ$. The differential cross sections are presented as a function of the number of field periods (T) elapsed during the propagation. At the final time of $10T$ we compare our calculations with the ECS calculations of Vanroose *et al* [12] (red dashed line).

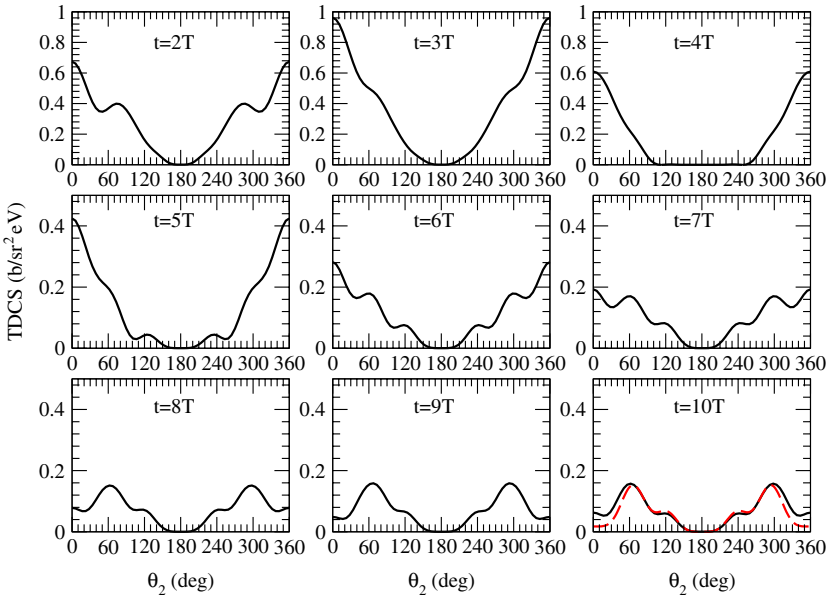

Figure 6. Triple differential cross sections for H_2 for $E_1 = E_2 = 12.5$ eV, for $\theta_1 = 0^\circ$, and for $\theta_N = 0^\circ$. The differential cross sections are presented as a function of the number of field periods (T) elapsed during the propagation. At the final time of $10T$ we compare our calculations with the ECS calculations of Vanroose *et al* [12] (red dashed line).

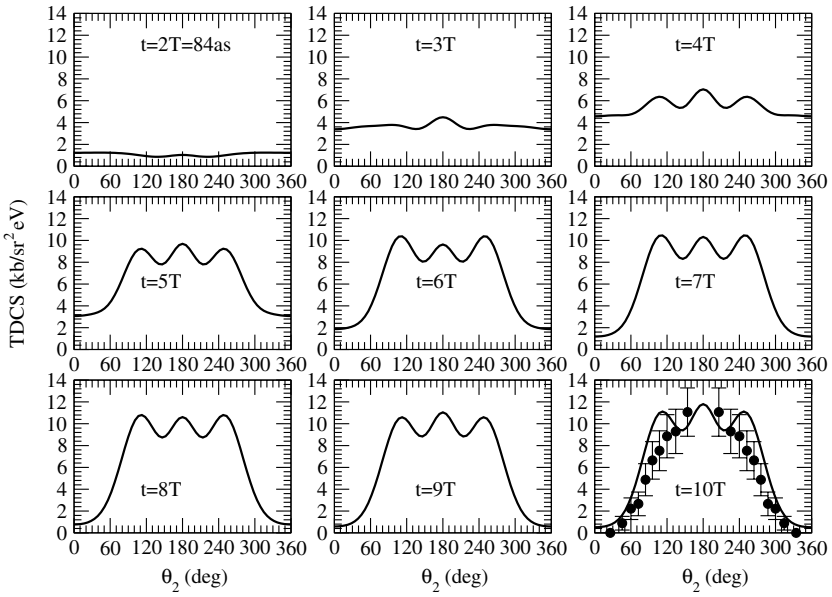

Figure 7. Triple differential cross sections for He for $E_1 = 17$ eV, $E_2 = 3$ eV, for $\theta_1 = 0^\circ$. The differential cross sections are presented as a function of the number of field periods (T) elapsed during the propagation. The first cross sections are computed after 84 attoseconds (as) as indicated. At the final time of $10T$, we compare our calculations with the measurements of Bräuning *et al* [10].

compared with time-independent ECS calculations [12], where excellent agreement is found. The magnitude of the cross section also increases until around $5T$, after which it is quite stable.

The cross sections shown in figure 6, where $\theta_N = 0^\circ$, show some similar patterns to figure 5. Again, selection rules give a 'hard' zero in the cross section at $\theta_2 = 180^\circ$, and the zero at $\theta_2 = 0^\circ$ takes some time to form. However, the cross sections for this geometry show a much richer structure, which is also observed in the time-independent ECS calculations, which reflect the nature of the molecular $M = 0 \rightarrow 0$ transition. It is also interesting that the magnitude of the cross section is actually greatest at early times, and that the cross section settles down to a converged value which is 50% lower than the cross-section magnitude at early times. Again this is also observed in the development of the total cross section as a function of time, for this transition. This behaviour is quite different from the He case and for the $M = 0 \rightarrow 1$ transition.

It is also possible to extract the triple differential cross sections as a function of time for unequal energy sharing electrons, where fewer selection rules exist than at equal energy sharing. In figure 7 we examine once more the He double photoionization at $\theta_1 = 0^\circ$, where in this case electron 1 has 17 eV of the available excess energy of 20 eV. The near-zero at $\theta_2 = 0^\circ$ again takes some time to evolve, and the cross section has reached a stable value after 7 or 8 field periods. Again, the final stable cross section value is in very good agreement with the measurements of Bräuning *et al* [10]. The peak in the cross section at $\theta_2 = 180^\circ$, now no longer forbidden, quickly forms after only a few field periods. Before this, the cross section is relatively flat, which may reflect the early dominance of lower partial waves in the double ionization, which are more isotropic. For the corresponding H_2 case shown in figure 8, where $\theta_N = 90^\circ$ and $E_1 = 22$ eV (of an available excess energy of 25 eV), the dominant peak at $\theta_2 = 180^\circ$ quickly forms, and again the near-zero in the cross section at $\theta_2 = 0^\circ$ takes around

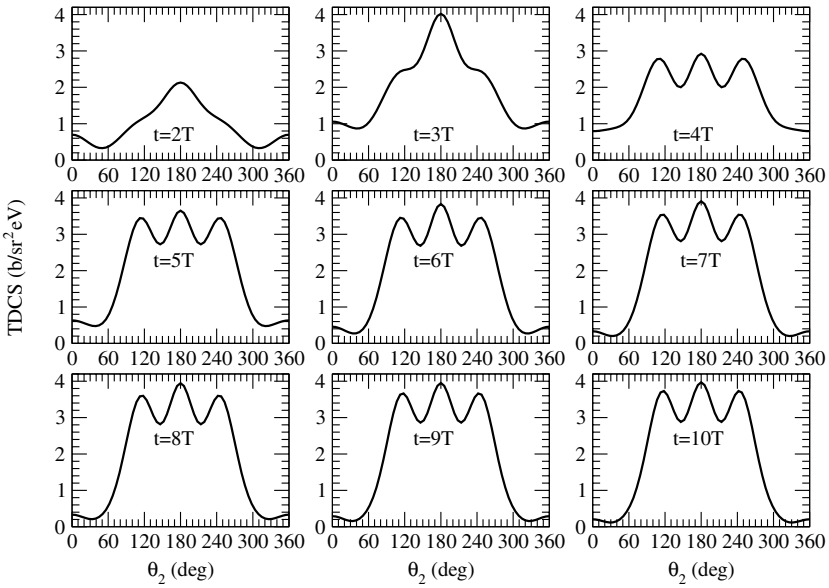

Figure 8. Triple differential cross sections for H_2 for $E_1 = 22$ eV, $E_2 = 3$ eV, for $\theta_1 = 0^\circ$ and for $\theta_N = 90^\circ$. The differential cross sections are presented as a function of the number of field periods (T) elapsed during the propagation.

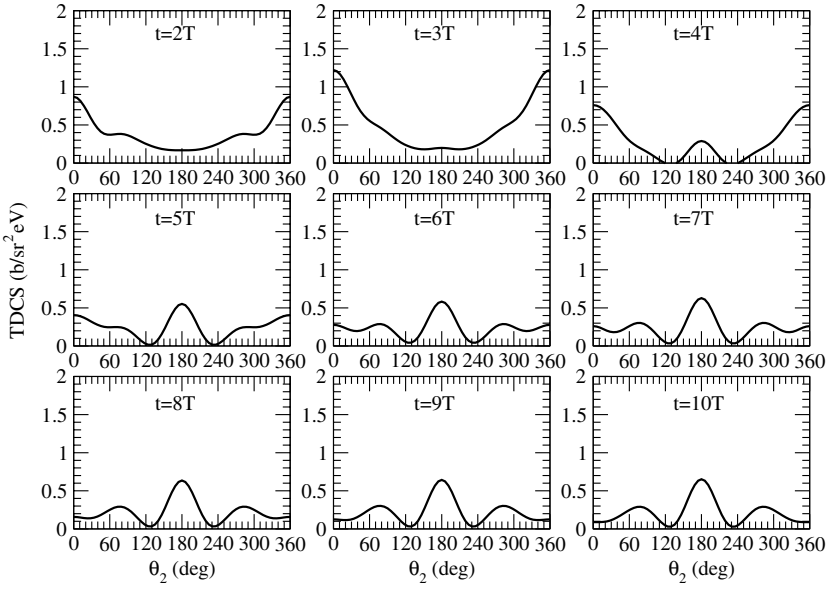

Figure 9. Triple differential cross sections for H_2 for $E_1 = 22$ eV, $E_2 = 3$ eV, for $\theta_1 = 0^\circ$ and for $\theta_N = 0^\circ$. The differential cross sections are presented as a function of the number of field periods (T) elapsed during the propagation.

7 or 8 field periods to form. The similarities in the final shape of the triple differential cross sections for this geometry with the He case are clear.

Finally, in figure 9 we examine the same unequal energy sharing conditions as in figure 8, but again for $\theta_1 = 0^\circ$. As found in figure 6, the cross section is actually largest at early times, with the final peak in the cross section at $\theta_2 = 180^\circ$ not dominant until after 6 field periods. Still, after around 8 field periods, the triple differential cross sections are quite stable.

4. Conclusions

This study of the evolution of the triple differential cross sections for He and for H_2 has highlighted some similarities in the photoionization process between the two systems. For example, the shapes of the differential cross sections for He and for H_2 when the molecule is at 90° to the polarization axis are quite similar at most of the times during the photoionization process. However, when the molecule is at 0° to the polarization axis, the triple differential cross section behaves quite differently as a function of time. The magnitude is large at early times and then decreases to a constant value. The shapes of the triple differential cross section also have more structure compared with the cross section when the molecule is at 90° to the polarization axis. Arbitrary orientations of the molecular axis with respect to the polarization axis will contain components of the $M = 0$ and $M = 1$ amplitudes.

We also find that the triple differential cross sections tend to converge to a stable value after 7 or 8 field periods. This will depend on the excess energy of the outgoing electrons; as discussed in detail previously [24], at energies closer to threshold, the double ionization cross sections take longer to converge. Furthermore, we have found that the convergence of the shape of the angular distributions is highly dependent on the electron–electron interaction terms; for distributions where the electrons can be expected to interact strongly, the shape of the distribution takes longer to form a stable value.

It is interesting to speculate if the distributions presented in figures 3–9 could be observed by experiment. The formation of the triple differential cross sections takes place over a time of a few hundred attoseconds, which is almost within the range of the latest generation of short pulse lasers. By using such lasers to 'freeze' or image the motion of the electrons as they distribute themselves after ionization by a much longer (synchrotron) pulse of light, it may be possible to watch the angular distributions take shape. Such a feat would be a stunning confirmation of the ability to control matter using light at the most detailed level possible.

Acknowledgments

A portion of this work was performed under the auspices of the US DOE through Los Alamos National Laboratory and through a grant to Auburn University, as well as an NSF grant to Auburn University. Computational work was carried out at the National Center for Computational Sciences in Oak Ridge, TN, and at Los Alamos National Laboratory.

References

[1] Kheifets A S and Bray I 1998 *J. Phys. B: At. Mol. Opt. Phys.* **31** L447–53
[2] Kheifets A S and Bray I 2000 *Phys. Rev.* A **62** 065402
[3] Malegat L, Selles P and Kazansky A K 2000 *Phys. Rev. Lett.* **85** 4450–3
[4] Selles P, Malegat L and Kazansky A K 2002 *Phys. Rev.* A **65** 032711
[5] Pindzola M S and Robicheaux F 1998 *Phys. Rev.* A **57** 318–24
[6] Colgan J, Pindzola M S and Robicheaux F 2001 *J. Phys. B: At. Mol. Opt. Phys.* **34** L456–66
[7] Colgan J and Pindzola M S 2002 *Phys. Rev.* A **65** 032729
[8] McCurdy C W, Horner D A, Rescigno T N and Martín F 2004 *Phys. Rev.* A **69** 032707
[9] Horner D A, Colgan J, Martín F, McCurdy C W, Pindzola M S and Rescigno T N 2004 *Phys. Rev.* A **70** 064701

[10] Bräuning H *et al* 1998 *J. Phys. B: At. Mol. Opt. Phys.* **31** 5149–60
[11] Vanroose W, Martín F, Rescigno T N and McCurdy C W 2005 *Science* **310** 1787–9
[12] Vanroose W, Horner D A, Martín F, Rescigno T N and McCurdy C W 2006 *Phys. Rev.* A **74** 052702
[13] Colgan J, Pindzola M S and Robicheaux F 2007 *Phys. Rev. Lett.* **98** 153001
[14] Weber T *et al* 2004 *Phys. Rev. Lett.* **92** 163001
[15] Weber T *et al* 2004 *Nature* **431** 437–41
Weber T *et al* 2006 *Nature* **443** 1014
[16] Gisselbrecht M, Lavolee M, Huetz A, Bolognesi P, Avaldi L, Seccombe D P and Reddish T J 2006 *Phys. Rev. Lett.* **96** 153002
[17] Vanroose W, Martín F, Rescigno T N and McCurdy C W 2004 *Phys. Rev.* A **70** 050703
[18] Colgan J, Pindzola M S and Robicheaux F 2004 *J. Phys. B: At. Mol. Opt. Phys.* **37** L377–84
[19] Horner D A, Vanroose W, Rescigno T N, Martín F and McCurdy C W 2007 *Phys. Rev. Lett.* **98** 073001
[20] Pindzola M S and Robicheaux F 1998 *J. Phys. B: At. Mol. Opt. Phys.* **31** L823–31
[21] Colgan J and Pindzola M S 2002 *Phys. Rev. Lett.* **88** 173002
[22] Maulbetsch F and Briggs J S 1995 *J. Phys. B: At. Mol. Opt. Phys.* **28** 551–64
[23] Knapp A *et al* 2002 *Phys. Rev. Lett.* **89** 033004
[24] Kleiman U, Pindzola M S and Robicheaux F 2005 *Phys. Rev.* A **72** 022707